Estimating normal effective stress degradation in sand under undrained simple shear condition

Ze-Xiang WU[1,2,3], Christophe DANO[4], Pierre-Yves HICHER[3], Zhen-Yu YIN[2*]

[1] College of Architecture and Civil Engineering, Wenzhou University, Wenzhou, China;

[2] Department of Civil and Environmental Engineering, The Hong Kong Polytechnic University, Hong kong, China;

[3] Research Institute of Civil Engineering and Mechanics (GeM), UMR CNRS 6183, Ecole Centrale de Nantes, Nantes, France;

[4] Université Grenoble Alpes, CNRS, Grenoble INP, 3SR, Grenoble, France;

[*]Corresponding Author. Email: zhenyu.yin@gmail.com

Abstract:

The degradation of the effective normal stress in soil surrounding the pile caused by undrained cyclic loading affects the shaft capacity of the pile and can lead to structural instability. In order to investigate this phenomenon, a series of constant volume monotonic and cyclic simple shear tests on Fontainebleau sand has been conducted. Based on the experimental results, the shear stress at phase transformation state is firstly determined for different initial void ratios and initial normal effective stresses. Then, the number of cycles to liquefaction is estimated as a function of both the cyclic and the average shear stresses normalized by the shear stress at phase transformation. An empirical equation to evaluate the normal stress degradation is formulated and the procedure of parameter identification is presented. The performance of the suggested formulation has been analyzed, based on simple shear test results on Fraser River sand and Quiou sand, and triaxial tests on Karlsruhe sand, and it has been validated by a series of additional tests on Fontainebleau sand. All the results indicate that the proposed formulation is able to estimate with good accuracy the effective normal stress degradation in sand subjected to undrained cyclic shearing.

Keywords: normal stress degradation; sand; simple shear; cyclic loading; phase transformation; cyclic resistance

1. Introduction:

Pile foundations are generally subjected to lateral and axial, monotonic and cyclic loads, as for example is the case for wind turbines. Because the severity of the loads can induce a degradation of the shaft capacity (Andersen 2009; Gavin et al. 2011), in particular of the axial cyclic components, it needs to be more deeply investigated. Indeed, the initial horizontal effective stress at the interface between the soil and the pile, governing the level of the local shear resistance and thus the global shaft capacity, could be gradually reduced due to the generation of excess pore pressure during cyclic loading. Therefore, it is highly valuable to develop analytical methods which address the changes of the soil properties so that the evolution of the shaft capacity of piles under cyclic loading can be more easily interpreted.

Field and laboratory model pile tests have been performed to understand the evolution of the shaft capacity during pile installation and service conditions inducing cyclic axial loading (Jardine et al. 2000 and 2005; Yang et al. 2010; Jardine and Standing 2012; Tsuha et al. 2012; Pra-Ai 2013; Aghakouchak et al. 2015). Full-scale pile tests subjected to axial cyclic loading performed by Jardine et al. (2000) demonstrated that high-level cyclic loading can be highly detrimental to shaft capacity. In laboratory conditions, tests using the mini-ICP (Imperial College Pile) model pile installed in a pressurized calibration chamber (Yang et al. 2010; Tsuha et al. 2012) have also provided key information for improving the modeling of pile-soil interaction and the design rules. Based on their recent works on the degradation of shaft capacity in model pile tests, Jardine et al. (2005) and Aghakouchak et al. (2015) have suggested an empirical "ABC" formulation involving the shaft cyclic shear stress (τ_{cyc}) normalized by the maximum static shear stress $\tau_{max,static}$ and the number of cycles (N):

$$\frac{\Delta\sigma'_n}{\sigma'_{n0}} = A \cdot \left[B + \frac{\tau_{cyc}}{\tau_{\max,static}} \right]^C \cdot \log_{10}(N) \quad (1)$$

where σ'_{n0} is the initial effective normal stress to the shaft and $\Delta\sigma'_n$ the variation (degradation) of the

normal effective stress. A, B and C are three constant empirical values which can be identified through back-analysis of pile tests or through calibration from laboratory experiments. However, the influence of the mean shear stress τ_{ave} has not been introduced in the "ABC" model (Tsuha et al. 2012).

Similarly, in order to investigate the soil response under cyclic loading, various cyclic tests such as triaxial tests, simple or direct shear tests, torsional shear tests (Hyodo et al. 1991; Yoshimine et al. 1998 and 1999; Vaid et al. 2001; Andersen 2009; Jin et al., 2015; Aghakouchak et al. 2015; Yin et al., 2010, 2013, 2018; Qian et al., 2016, 2018), have also been conducted, usually by assuming uniform load-controlled cycles on the specimen in undrained conditions. Based on these soil element tests, various empirical equations have been proposed for predicting the soil response concerning the generation of pore pressure or the degradation of the effective normal stress. Based on cyclic triaxial tests, Seed and Idriss (1971) have defined a uniformed 'S' shape for the generation of excess pore pressure which can be formulated by an arcsine function depending on a normalized number of cycles to liquefaction (Mitchell and Dubin 1986; Polito et al. 2008; Wang et al. 2013a; Mohtar et al. 2014; Porcino et al. 2015). Ishibashi et al. (1977) have developed a model of incremental pore pressure depending on the shear stress amplitude and the number of cycles (Sherif et al. 1978; Ishibashi et al. 1982; Krishnaswamy and Thomas Isaac 1995; Georgiannou and Tsomokos 2008; Wang et al. 2013b; Konstadinou and Georgiannou 2014). Nemat-Nasser and Shokooh (1979) have introduced an 'energy-based' method in which the generation of excess pore pressure is related to the amount of dissipated energy (shear work) during cyclic loading (Towhata and Ishihara 1985; Law et al. 1990; Green et al. 2000; Dief and Figueroa 2007). Note that the influence of the initial average shear stress, which is however known as a key factor to enhance the cyclic resistance of sand (Vaid and Chern 1983; Vaid et al. 2001; Yang and Sze 2011; Gu et al. 2016; Yang and Pan 2017), has not been considered in these predictive models. Hence, a more efficient approach for describing more precisely the degradation of the effective normal stresses acting on a pile shaft must include the investigation of the influence of the initial average shear stress.

Until now, only laboratory experiments have been considered to quantify the degradation of the

effective normal stress due to shearing. Most experimental studies have limited this scope on results from triaxial tests. In spite of their shortcomings (Andersen 2009), simple shear tests have been preferred to triaxial tests since the interface shearing is much better reproduced through this type of testing, even if direct shear testing could also be considered (Pra-ai 2013; Wang et al 2016; Pra-ai and Boulon 2017). Similarly, even if it is now currently accepted that the shearing of a soil–pile interface occurs at a relatively constant normal stiffness (Fakharian and Evgin 1997), a conservative approach would be to in perform constant volume simple shear tests, which maximizes the degradation of the effective normal stress, as previously done in (Lambe and Whitman 1969; Dyvik et al. 1987; Andersen 2009) for instance. The stress state of a soil element around the pile foundation is shown in Figure 1. The soil element is subjected to cyclic loading with symmetrical loading ($\tau_{ave} = 0$) or non-symmetrical loading ($\tau_{ave} \neq 0$).

From the above literature review, the following points could be noted. Firstly, in the laboratory, soil element tests would greatly simplify the testing operation and reduce significantly the financial cost compared to full size or even model pile tests for studying the soil response during cyclic loading. Secondly, the effect of the initial average shear stress is rarely investigated. Thirdly, compared with triaxial tests, simple shear tests are acknowledged to provide more representative loading conditions for interface shearing.

This study, therefore, aims to provide a contribution to characterize the degradation of the effective normal stress based on undrained monotonic and cyclic simple shear tests on Fontainebleau sand and to develop a procedure for calibrating this degradation. Following these objectives, the first task was to determine by undrained monotonic simple shear tests the phase transformation line (PTL), since the position of the PTL governs the volumetric behavior and, therefore, the pore pressure evolution. Then, the number of cycles to liquefaction was investigated based on the results of cyclic simple shear tests under different loading conditions. Furthermore, an empirical formulation expressing the degradation of the effective normal stress during cyclic loading was developed. Then, experimental data on Fraser River sand and a carbonate sand from Quiou (France) obtained through

simple shear tests on the one hand, and on Karlsruhe sand subjected to triaxial loading on the other hand, were selected from the literature review to verify the proposed calibration procedure. Finally, a series of additional tests were performed on Fontainebleau sand in order to verify the accuracy of the proposed empirical equation.

2. Material and testing program

The tested material is the Fontainebleau sand NE34, a fine siliceous sand with sub-rounded grains (Figure 2a). Its main characteristics, summarized in Table 1, are a mean grain size of about 210 µm, a coefficient of uniformity of 1.53, minimum and maximum void ratios of 0.510 and 0.882, respectively, a specific weight of 26.00 kN/m^3 (Andria-Ntoanina et al. 2010). As a reference material in France for geotechnical applications, this sand has been used in many experimental studies. Its cyclic behavior has been relatively well documented at the scale of the representative elementary volume in laboratory tests as well as at the scale of soil–structure interactions (Dupla and Canou 1994; Gaudin et al. 2005; Yang et al. 2010; Gu et al. 2014; Pra-ai and Boulon 2017), resulting in the establishment of the Poulos cyclic stability diagram (Poulos 1988).

The simple shear device used in this study is a commercial apparatus whose design is close to the NGI simple shear apparatus (Bjerrum and Landva 1966). The servo-controlled system is capable of conducting stress or strain controlled loading paths in both horizontal and vertical directions (Figure 1). An air-pluviation technique was developed to prepare the specimens, as shown in Figure 2(b), in which the sand is deposited from a predetermined height into the specimen mold in order to obtain a predetermined relative density. For sands, the cylindrical reconstituted specimens, 70 mm in diameter and 25 mm in height (ratio of 0.36 to minimize the effects of friction on the lateral sides), were prepared by air-pluviation, which is considered to approximate the natural deposition process (Vaid and Negussey 1984). The specimens are confined in a soft butyl membrane with a thickness of 0.2 mm, itself placed against a stack of rigid circular Teflon-coated thin rings (1 mm each) which maintains a constant cross-sectional area but allowed simple shear deformation (Figure 2c). On both sides, the

sand is in contact with rough sintered stainless steel plates to prevent any sliding between the pedestals and the specimen. The constant volume condition is ensured by constraining the height of the sample to a constant value after the K_0-consolidation. Compared to a truly undrained test where the evolution of excess pore pressure can be directly measured, the normal effective stress σ'_n on the horizontal plane continuously varies to fulfill the constant volume condition during simple shear testing. The assumption that the change in the applied normal effective stress is equal to the excess pore which would have developed in a truly undrained test has been validated by Dyvik et al. (1987), and has been applied in extensive laboratory testing during the last two decades.

The experimental campaign consisting of monotonic and cyclic simple shear tests is presented in Table 2. For the cyclic tests, sine cycles with a frequency of 0.05 Hz were applied. The dry specimens were first consolidated under K_0-condition up to a given initial effective normal stress σ'_{n0}. Three series of constant volume simple shear tests were carried out:

1) The first series consisted of monotonic simple shear tests, which were performed at different initial effective normal stresses ($104 \leq \sigma'_{n0} \leq 416$ kPa) and different void ratios after consolidation ($0.59 \leq e_0 \leq 0.74$). The objective of this part was to determine the shear stress at phase transformation state τ_{pt}, for different void ratios after consolidation e_0 and different initial effective normal stresses σ'_{n0}.

2) The second series consisted of symmetrical cyclic simple shear tests (the average shear stress τ_{ave} was null). Several tests with different cyclic shear stress amplitudes ($5.2 \leq \tau_{cyc} \leq 62.4$ kPa) and initial normal stresses ($104 \leq \sigma'_{n0} \leq 416$ kPa) on medium dense specimens were performed. The objective of this part was to study the influence of the cyclic shear stress τ_{cyc} on the number of cycles to liquefaction N_L.

3) The third series consisted of non-symmetrical cyclic simple shear tests ($\tau_{ave} \neq 0$), with different cyclic shear stress amplitudes ($10.4 \leq \tau_{cyc} \leq 41.6$ kPa) and different average shear stresses ($5.2 \leq \tau_{ave} \leq 41.6$ kPa) on medium dense specimens under an effective normal stress $\sigma'_{n0} = 416$ kPa.

Two sets of loading conditions, namely shear stress-reversal ($\tau_{cyc} > \tau_{ave}$) and no shear stress-reversal ($\tau_{cyc} \leq \tau_{ave}$), were applied. The objective in this part was to study the influence of the average shear stress τ_{ave} on the number of cycles to liquefaction N_L.

3. Test results and interpretation

3.1. Monotonic stress-strain behavior

Figure 3 shows the stress-strain response of Fontainebleau sand samples during monotonic simple shear testing. The shear strain γ is defined as $\gamma = \Delta d/H_0$ (where H_0 is the sample height at the start of the shearing, and Δd is the horizontal displacement). Under constant volume condition, the shearing-induced, at first, a decrease of the effective normal stress before the phase transformation state was reached. The extreme points in the shear stress–effective normal stress diagram mark the change from contractancy to dilatancy and therefore the position of the phase transformation state. Beyond that state, the effective normal stress increased towards the failure line. Figure 3(a, b) presents the influence of the void ratio after consolidation e_0 for a given effective normal stress of 312 kPa. The loosest specimen after consolidation exhibits the largest decrease of the effective normal stress. Figure 3(c, d) presents the influence of the initial effective normal stress level, from 104 kPa to 416 kPa, for a range of relative densities corresponding to a medium density. The friction angle at failure ϕ_f is equal to 30°. The phase transformation states are located on a unique straight line passing through the origin, whose slope corresponds to a friction angle of 24°. The phase transformation line (PTL) delineates two distinct volumetric behaviors (contractancy below PTL, dilatancy between PTL and failure line), which will subsequently govern the evolution of the samples during cyclic shearing. In Figure 3(e,f), the effective normal stress (σ'_n) and the shear stress (τ) are normalized by the corresponding initial effective normal stress (σ'_{n0}) and the shear stress at phase transformation state (τ_{pt}), respectively. For the same initial effective normal stress, a smaller void ratio e_0 corresponds to a larger normalized effective normal stress ($\sigma'_{n\text{-}pt}/\sigma'_{n0}$) at the phase transformation state. For the same void ratio, the magnitude of the normalized stress at the phase

transformation state ($\sigma'_{n\text{-}pt}/\sigma'_{n0}$, τ/τ_{pt}) is slightly affected by the value of the initial effective normal stress.

The values of the shear stress at phase transformation τ_{pt} are plotted in Figure 4a against the relative density after consolidation D_{r0}, defined in Eq. 2. It can be seen that the shear stress τ_{pt} depends on the void ratio e_0 and on the initial normal effective stress σ'_{n0}. In Figure 4b, the shear stress τ_{pt} is normalized by the initial effective normal stress σ'_{n0} and plotted as a function of D_{r0}. A non-linear relationship between the void ratio e_0 and the normalized shear stress τ_{pt}/σ'_{n0} is obtained and an empirical function can be deduced, which allows us to estimate the shear stress τ_{pt}, depending on the given parameters σ'_{n0} and e_0 (Eq. 2). The parameters α and β were calibrated by fitting the experimental data for Fontainebleau sand: $\alpha = 0.68$ and $\beta = 1.76$.

$$\tau_{pt} = \alpha \cdot \sigma'_{n0} \cdot \tan\phi_{pt} \cdot D_{r0}^{\beta} \quad \text{with} \quad D_{r0} = \frac{e_{max} - e_0}{e_{max} - e_{min}} \tag{2}$$

3.2. Symmetrical cyclic loading

13 constant volume symmetrical cyclic simple shear tests were performed on medium dense Fontainebleau sand specimens under various initial effective normal stresses (σ'_{n0} = 104, 208, 312, 416 kPa). A typical test result (Test c21: $\tau_{ave} = 0$ kPa, $\tau_{cyc} = 20.8$ kPa, $\sigma'_{n0} = 416$ kPa) is presented in Figure 5. Upon reaching the phase transformation line, the effective stress path started to follow a butterfly-shaped loop due to the continuous transition from contractany to dilatancy. It also quickly approached the failure line, which resulted in a rapid generation of large shear strains (Figure 5a, b and c). The effective normal stress σ'_n decreased with the number of cycles, until reaching a minimum value ($\sigma'_n \approx 0$ kPa) when liquefaction occured (Figure 5d). Under this condition, the specimen could no longer sustain any loading (loss of controllability of the test). In this example, the required number of cycles to trigger liquefaction N_L was equal to 62 (N_L = 62). For the undrained cyclic loading, due to the volume change not occurring, the stress-dilatancy relationship associates with the change of effective normal stress. The sand undergoing a degradation of σ'_n is firstly subjected

to an over-consolidation state until the stress state exceeds the phase transformation stress state where the volumetric strain increment changes from contractive to dilative behaviour. Then, the sand enters the stage of cyclic mobility.

The degradation of the effective normal stress for all the symmetrical cyclic tests has been compiled in Figure 6, as a function of the initial normal effective stress σ'_{n0} and for different cyclic shear stresses τ_{cyc}. As expected, for a given effective initial normal stress, the number of cycles to liquefaction increased as the cyclic shear stress decreased. Likewise, a higher initial effective normal stress delayed the occurrence of liquefaction (greater N_L) since the distance between the initial stress state and the corresponding phase transformation state in the (σ'_{n0} - τ) stress plane was larger. In order to establish a correlation between the cyclic shear stress and the number of cycles to liquefaction, the cyclic shear stress amplitude was normalized by the phase transformation shear stress τ_{pt} obtained through monotonic simple shear tests and calculated by Eq. (2). The results (points in Figure 7) are plotted versus the number of cycles to liquefaction N_L. The experimental data are then fitted assuming a power function between N_L and the normalized cyclic shear stress ratio τ_{cyc}/τ_{pt}, as indicated in Eq. 3. In the case of Fontainebleau sand, the power ζ was found equal to 0.27.

$$\frac{\tau_{cyc}}{\tau_{pt}} = \frac{1}{N_L^{\zeta}} \quad (3)$$

3.3. Non-symmetrical cyclic loading

14 constant volume non-symmetrical cyclic simple shear tests were performed on medium dense Fontainebleau sand samples with a given initial normal effective stress (σ'_{n0} = 416 kPa). Two loading conditions were imposed: stress reversal ($\tau_{cyc} > \tau_{ave}$) and no-stress reversal ($\tau_{cyc} < \tau_{ave}$) cyclic loading. Figure 8 shows a typical test result (Test c29) for stress reversal cyclic loading (τ_{cyc} = 20.8 kPa, τ_{ave} = 10.4 kPa, σ'_{n0} = 416 kPa). The response was very similar to the one observed in the symmetrical case, except for a small evolution of the average shear strain. The comparison of Figures 5 and 8, for which the unique difference is the value of the average shear stress (0 kPa for Test c21 in Figure 5,

10.4 kPa for Test c29 in Figure 8), demonstrates that an increase of the average shear stress favors the degradation of the effective normal stress, since the number of cycles to liquefaction was reduced by a factor of about 1/3 (62 to 39 cycles). Similarly, a typical result of no-stress reversal cyclic loading (Test c39: τ_{cyc} = 20.8 kPa, τ_{ave} = 41.6 kPa, σ'_{n0} = 416 kPa) is reported in Figure 9. All the test loading conditions except the value of the average shear stress were the same, as in Tests c21 and c29 previously discussed. The instability, corresponding to a cyclic mobility mechanism, occurred at a smaller number of cycles (between 15 and 20 cycles), due to the proximity of the stress path to both the PT and failure lines. The effective normal stress reached a residual value (100 kPa in the case of Test c39). For this type of test, the instability was determined by the condition of the effective normal stress reaching a residual value ($\sigma'_{n\text{-residual}}$ = 98 kPa).

Figure 10 summarizes all the results relative to non-symmetrical cyclic tests under the same initial effective normal stress of 416 kPa with different average shear stresses. The results corresponding to the stress reversal condition for which the effective normal stresses decreased to zero, i.e. the liquefied state, were plotted in red. For the no-stress reversal condition, the effective normal stress decreased to a residual stress. For a better comparison of the results obtained under these two conditions, the number of cycles to instability (liquefaction or cyclic mobility) was defined by the effective normal stress reaching the limited final value. The degradation of the effective normal stress for all the non-symmetrical cyclic tests was plotted as a function of the cyclic shear stress τ_{cyc} and the average shear stress τ_{ave} in Figure 10. As expected, for a given average shear stress, the number of cycles to liquefaction increased with the decrease of the cyclic shear stress.

Figure 11(a) presents the hysteresis loops of non-stress reversal cyclic loading corresponding to the cyclic mobility final state which were used to calibrate the value of the residual effective normal stress ($\sigma'_{n\text{-residual}}$). The values of $\sigma'_{n\text{-residual}}$ corresponding to the maximum shear stress τ_{max} which is equal to the average shear stress τ_{ave} plus the cyclic shear stress τ_{cyc}, are shown in Figure 11(b) for nine no-stress reversal cyclic tests. An empirical expression could be suggested to evaluate the residual effective normal stress:

$$\sigma'_{\text{n-residual}} = \begin{cases} \chi \cdot \tau_{\max} \cdot \tan^{-1}(\phi_f) & ;(\tau_{ave} \geq \tau_{cyc}) \\ 0 & ;(\tau_{ave} < \tau_{cyc}) \end{cases} \quad (4)$$

where χ is a parameter obtained by fitting the data of non-stress reversal cyclic tests (χ = 0.77 for Fontainebleau sand); $\tau_{\max}$ is the maximum shear stress equal to $\tau_{ave}+\tau_{cyc}$; ϕ_f is the friction angle at failure. A good agreement could be obtained between calculated results (dash blue line) and measurements (red symbols).

4. Evaluation of the degradation of the effective normal stress

4.1. Number of cycles to liquefaction

The experimental data were mapped on a 3D plot, where two axes represent the stress ratios τ_{cyc}/τ_{pt} and τ_{ave}/τ_{pt}, and the third one, the number of cycles to instability (liquefaction or cyclic mobility) (Figure 12). This plot can be used to describe the cyclic resistance of Fontainebleau sand. For a constant level of normalized average shear stress (τ_{ave}/τ_{pt}), the number of cycles to instability decreases with the increase of the normalized cyclic shear stress (τ_{cyc}/τ_{pt}). Inversely, for a constant level of normalized cyclic shear stress (τ_{cyc}/τ_{pt}), the number of cycles to instability decreases with the increase of the normalized average shear stress (τ_{ave}/τ_{pt}).

In order to formulate an expression for the number of cycles to instability, all the couples of normalized stresses (τ_{ave}/τ_{pt}, τ_{cyc}/τ_{pt}) were reported in a diagram of stability shown in Figure 13(a). The space is then delimited by the diagonal corresponding to a failure at the first cycle. Instabilities reached at a higher number of cycles N_L fell on straight lines whose slope K decreased with N_L, as shown in Figure 13 (a). The slope K can be approximated by:

$$K = \frac{\tau_{cyc}/\tau_{pt}}{1-\tau_{ave}/\tau_{pt}} = \frac{\tau_{cyc}}{\tau_{pt}-\tau_{ave}} \quad (5)$$

Figure 13 (b) correlates the calculated values of K and the corresponding values of N_L which can

be expressed by:

$$N_L = \mu \cdot \left(\frac{\tau_{cyc}}{\tau_{pt} - \tau_{ave}} \right)^{-\psi} \quad (6)$$

where μ and ψ are parameters obtained by fitting the experimental results (μ = 1.396, ψ = 3.505 for Fontainebleau sand).

The diagram in Figure 13(a) can be used to predict the number of cycles to instability (Jardine et al. 2005; Tsuha et al. 2012). The influence of the average shear stress and of the cyclic shear stress has been taken into account in Eq. (5), whereas the link between cyclic and monotonic responses of sand is obtained by the variable τ_{pt} calibrated by Eq. (2), the function of the void ratio e and of the initial effective normal stress σ'_{n0}.

4.2. Degradation of effective normal stress

During stress-controlled constant volume cyclic simple shear testing, the effective normal stress σ'_n decreases from its initial value either to zero or to a residual value. In agreement with the empirical expression of the pore pressure evolution suggested by ~~Seed and Booker~~ Seed and Idriss (1971), the degradation of the effective normal stress can be expressed by the following relation:

$$\frac{\sigma'_n - \sigma'_{n-residual}}{\sigma'_{n0} - \sigma'_{n-residual}} = \frac{2}{\pi} \arccos\left(\frac{N}{N_L} \right)^{\frac{1}{\theta}} ; \quad \left(if \ \ \tau_{ave} < \tau_{cyc}, \sigma'_{n-residual} = 0 \right) \quad (7)$$

where N is the current number of cycles and θ is a material parameter.

To identify the material parameter θ, the effective normal stress σ'_n normalized by its initial value σ'_{n0} was represented as a function of the normalized number of cycles to instability (N/N_L), as shown in Figure 14. 6 experimental results (Tests c19, c20, c23, c26, c28 and c32) with different initial effective normal stresses, different cyclic shear stresses and different average shear stresses were selected to verify the empirical equation. The fitting of Eq. 7 with experimental data led to a

value θ=3.4 for Fontainebleau sand. By combining Equations 6 and 7, the following relationship can be proposed:

$$\frac{\sigma'_n - \sigma'_{n-residual}}{\sigma'_{n0} - \sigma'_{n-residual}} = \frac{2}{\pi} \cdot \arccos\left(\frac{1}{\mu} \cdot N \cdot \left(\frac{\tau_{cyc}}{\tau_{pt} - \tau_{ave}} \right)^{\psi} \right)^{\frac{1}{\theta}} \quad (8)$$

where $\sigma'_{\text{n-residual}}$ = 0 kPa in the condition of cyclic stress reversal ($\tau_{\text{cyc}} > \tau_{\text{ave}}$) and $\sigma'_{\text{n-residual}}$ being calculated by using Eq. 4 in the condition of no-stress reversal ($\tau_{\text{cyc}} \leq \tau_{\text{ave}}$).

4.3. Calibration procedure

The calibration procedure for estimating the degradation of the normal effective stress is presented in Figure 15. Three successive steps are indicated in the calibration chart: (1) an expression of the shear stress at the phase transformation state needs be obtained according to the results of monotonic testing (Eq. 2); (2) a cyclic resistance diagram ($\tau_{\text{ave}}/\tau_{\text{pt}}$, $\tau_{\text{cyc}}/\tau_{\text{pt}}$, N_L) for predicting the number of cycles to liquefaction is plotted based on the cyclic test results (with different cyclic shear stresses and average shear stresses) in order to calibrate the parameters in Eq. 6; (3) the effective normal stress degradation is then calculated in order to calibrate Eqs. 7 and 8.

This analytical formulation can be easily used in practice to analyze the degradation of the shaft capacity for pile design. From this calibration procedure, a minimum of eight tests have to be considered for determining the material parameters, including at least 3 monotonic tests with different void ratios to determine the phase transformation state, 3 symmetrical cyclic loading tests with different cyclic stress amplitudes τ_{cyc} and 2 non-symmetrical cyclic loading tests with different average shear stresses τ_{ave} to study the degradation of the effective normal stress with the number of cycles.

In order to validate the whole procedure, simple shear tests on Fraser River sand (Sivathayalan 1994) and Quiou carbonate sand (Porcino et al. 2008), and triaxial tests on Karlsruhe sand

(Wichtmann and Triantafyllidis 2016a, 2016b) were selected. The physical properties of these three sands are presented in Table 3.

The normalized shear stresses at PTL (τ_{pt}/σ'_{n0} for simple shear tests and $q_{pt}/2p'_0$ for triaxial tests) were plotted against the corresponding relative densities in Figure 16. The curves of Eq. (2) as solid lines were fitted from the experimental data and the deduced parameters are given in Table 3. The cyclic stability diagram for calibrating the number of cycles to instability is shown in Figure 17. The parameters μ and ψ could be obtained by fitting the experimental results as shown in Table 4. Therefore, the behavior of different sands (quartz sand and carbonate sand) for different loading conditions (simple shear and triaxial loading) can be well expressed by Equations (2) and (6).

4.4. Validation of the suggested relationship

The calibration procedure has provided the following parameters for Fontainebleau sand: α = 0.68, β = 1.76, μ = 1.396, ψ = 3.505, θ=3.4. The tests presented in Table 2 can be considered as the training tests aimed to determine these parameters. 6 complementary tests with different loading conditions were selected and simulated to validate the performance of Eq. (8). As shown in Figure 18(a), the results can be well predicted for different loading conditions including symmetrical cyclic loadings with different τ_{cyc} (Tests c19, c20 and c23) and non-symmetrical cyclic loadings with different τ_{ave} (Tests c26, c28 and c32). To confirm the pertinence of this equation, a series of additional tests on Fontainebleau sand was performed at a consolidation stress level σ'_{n0} = 500 kPa with different loading paths including cyclic shear stresses from 12.5 kPa to 50 kPa and average shear stresses from 0 kPa to 50 kPa (Table 5). The results of these additional tests are presented in Figure 18(b), showing a behavior similar to the one obtained from the results of the training tests reported in Table 2. All additional tests were also simulated by Eq. (8) to verify the accuracy of the analytical method for predicting the mechanical behavior of a given sand. Figure 18(b) presents the comparison between the calculated effective normal stress (solid blue line) and the experimental data (red symbols). It demonstrates that Eq. (8) can successfully describe the evolution of the effective

normal stress for a large range of average shear stresses and cyclic shear stresses.

5. Conclusions

The aim of the paper has been to develop an analytical method for predicting the degradation of the effective normal stress of a soil element adjacent to a pile shaft under cyclic loading. The development of the analytical formulation was supported by a series of constant volume monotonic and cyclic simple shear tests performed on Fontainebleau sand specimens.

Monotonic simple shear tests on Fontainebleau sand with different void ratios and different initial normal effective stresses were firstly performed, allowing an empirical expression for calculating the shear stress at the phase transformation state to be suggested.

Then, cyclic simple shear tests were conducted under different initial effective normal stresses, cyclic shear stresses, and average shear stresses. Based on these experimental results, a cyclic resistance diagram was obtained, providing information concerning the number of cycles necessary to reach instability as a function of cyclic and average shear stress levels. The shear stress at the phase transformation state took into account the influence of void ratio and initial effective normal stress on the number of cycles to instability.

A calibration procedure for predicting the degradation of the effective normal stress was proposed. Following this procedure, an analytical expression to evaluate the normal effective stress degradation was developed with the following variables: void ratio, initial effective normal stress, cyclic shear stress, average shear stress and number of cycles. A series of additional tests including loading paths with different average shear stresses and cyclic shear stresses verified the proposed analytical expression. All comparisons between experimental results and simulations indicated that the proposed method is capable of predicting the degradation of the effective normal stress under constant volume cyclic shear loading.

Acknowledgments

The research described was supported by the French National Research Agency (ANR SOLCYP), the National Natural Science Foundation of China (51579179), and the Region Pays de la Loire of France (project RI-ADAPTCLIM).

Reference

Aghakouchak, A., Sim, W. W., & Jardine, R. J. (2015). Stress-path laboratory tests to characterise the cyclic behaviour of piles driven in sands. *Soils and Foundations, 55(5)*, 917-928.

Andersen, K. H. (2009). Bearing capacity under cyclic loading-offshore, along the coast, and on land. The 21st Bjerrum Lecture presented in Oslo, 23 November 2007 *Canadian Geotechnical Journal*, 46(5), 513-535.

Andria-Ntoanina, I., Canou, J., & Dupla, J. (2010). Caractérisation mécanique du sable de Fontainebleau NE34 à l'appareil triaxial sous cisaillement monotone. Laboratoire Navier–Géotechnique. CERMES, ENPC/LCPC.

Bjerrum, L., & Landva, A. (1966). Direct simple-shear tests on a Norwegian quick clay. *Géotechnique*, 16(1), 1-20.

Dief, H. M., & Figueroa, J. L. (2007). Liquefaction assessment by the unit energy concept through centrifuge and torsional shear tests. *Canadian Geotechnical Journal, 44(11)*, 1286-1297.

Dupla, J., & Canou, J. (1994). Caractérisation mécanique du sable de Fontainebleau apartir d'essais triaxiaux de compression et d'extension. *Rapport Interne CLOUTERRE II*, CERMES–ENPC.

Dyvik, R., Berre, T., Lacasse, S., & Raadim, B. (1987). Comparison of truly undrained and constant volume direct simple shear tests. *Géotechnique*, 37(1), 3-10.

Fakharian, K., & Evgin, E. (1997). Cyclic simple-shear behavior of sand-steel interfaces under constant normal stiffness condition. *Journal of Geotechnical and Geoenvironmental Engineering, 123(12)*, 1096-1105.

Gaudin, C., Schnaid, F., & Garnier, J. (2005). Sand characterization by combined centrifuge and laboratory tests. *International Journal of Physical Modelling in Geotechnics, 5(1)*, 42-56.

Gavin, K., Igoe, D., & Doherty, P. (2011). Piles for offshore wind turbines: a state of the art review. *Geotechnical Engineering, 164 (4)*, 245-256

Georgiannou, V., & Tsomokos, A. (2008). Comparison of two fine sands under torsional loading. *Canadian Geotechnical Journal, 45(12)*, 1659-1672.

Green, R., Mitchell, J., & Polito, C. (2000). An energy-based excess pore pressure generation model for cohesionless soils, *Proceedings of the John Booker Memorial Symposium*, 16-17.

Gu, C, Wang, J, Cai, Y.-Q & Guo, L. (2014) Influence of cyclic loading history on small strain shear modulus of saturated clays. *Soil Dynamics and Earthquake Engineering*. 66: 1-12

Gu, C, Wang, J, Cai, Y.-Q, Sun, L, Wang, P & Dong, Q.-Y (2016) Deformation characteristics of overconsolidated clay sheared under constant and variable confining pressure, Soils and Foundations, 56(3): 427-439.

Hyodo, M., Murata, H., Yasufuku, N., & Fujii, T. (1991). Undrained cyclic shear strength and

residual shear strain of saturated sand by cyclic triaxial tests. *Soils and Foundations, 31(3)*, 60-76.

Ishibashi, I., Sherif, M., & Tsuchiya, C. (1977). Pore-pressure rise mechanism and soil liquefaction. *Soils and Foundations, 17(2)*, 17-27.

Ishibashi, I., SHERIF, M. A., & CHENG, W.-L. (1982). The effects of soil parameters on pore-pressure-rise and liquefaction prediction. *Soils and Foundations, 22(1)*, 39-48.

Jardine, R., Chow, F., Overy, R., & Standing, J. (2005). *ICP design methods for driven piles in sands and clays*, Thomas Telford London.

Jardine, R., & Standing, J. (2012). Field axial cyclic loading experiments on piles driven in sand. *Soils and foundations, 52(4)*, 723-736.

Jardine, R., Standing, J., Health, & Safety Executive, L. (2000). Pile Load Testing Performed for HSE Cyclic Loading Study at Dunkirk, *France Volume 1. Offshore Technology Report-Health And Safety Executive Oto*.

Jin, Y.F., Yin, Z.-Y., Zhang, D.M., Huang, H.W. (2015). Unified modelling of monotonic and cyclic behaviours for sand and clay. Acta Mech. Solida Sin., 28(2): 111-132.

Konstadinou, M., & Georgiannou, V. (2014). Prediction of pore water pressure generation leading to liquefaction under torsional cyclic loading. *Soils and Foundations, 54(5)*, 993-1005.

Krishnaswamy, N., & Thomas Isaac, N. (1995). Liquefaction analysis of saturated reinforced granular soils. *Journal of geotechnical engineering, 121(9)*, 645-651

Lambe, T. W., & Whitman, R. V. (1969). Soil mechanics, series in soil engineering. *Jhon Wiley & Sons*.

Law, K. T., Cao, Y., & He, G. (1990). An energy approach for assessing seismic liquefaction potential. *Canadian Geotechnical Journal, 27(3)*, 320-329.

Mitchell, R. J., & Dubin, B. I. (1986). Pore pressure generation and dissipation in dense sands under cyclic loading. *Canadian Geotechnical Journal, 23(3)*, 393-398.

Mohtar, C. E., Bobet, A., Drnevich, V., Johnston, C., & Santagata, M. (2014). Pore pressure generation in sand with bentonite: from small strains to liquefaction. *Géotechnique, 64(2)*, 108.

Nemat-Nasser, S., & Shokooh, A. (1979). A unified approach to densification and liquefaction of cohesionless sand in cyclic shearing. *Canadian Geotechnical Journal, 16(4)*, 659-678.

Polito, C. P., Green, R. A., & Lee, J. (2008). Pore pressure generation models for sands and silty soils subjected to cyclic loading. *Journal of Geotechnical and Geoenvironmental Engineering, 134(10)*, 1490-1500.

Porcino, D., Caridi, G., & Ghionna, V. N. (2008). Undrained monotonic and cyclic simple shear behaviour of carbonate sand. *Géotechnique, 58 (8)*, 635-644.

Porcino, D., Marcianò, V., & Granata, R. (2015). Cyclic liquefaction behaviour of a moderately cemented grouted sand under repeated loading. *Soil Dynamics and Earthquake Engineering, 79*, 36-46.

Poulos, H. G. (1988). Cyclic stability diagram for axially loaded piles. *Journal of geotechnical engineering, 114(8)*, 877-895.

Pra-Ai, S. (2013). *Behaviour of soil-structure interfaces subjected to a large number of cycles*. Application to piles. Ph. D. thesis, Université de Grenoble.

Pra-Ai, S., & Boulon, M. (2017) Soil–structure cyclic direct shear tests: a new interpretation of the direct shear experiment and its application to a series of cyclic tests. *Acta Geotechnica, 12*, 107-127.

Qian, J.G., Wang, Y.G., Yin, Z.-Y., Huang, M.S. (2016). Experimental identification of plastic shakedown behavior of saturated clay subjected to traffic loading with principal stress rotation. Eng. Geol., 214: 29-42.

Qian, J.G., Du, Z.B., Yin, Z.-Y. (2018). Cyclic degradation and non-coaxiality of soft clay subjected to pure rotation of principal stress directions. Acta Geotech., 13(4): 943-959.

Seed, H. B., & Idriss, I. M. (1971). Simplified procedure for evaluating soil liquefaction potential. *Journal of Soil Mechanics & Foundations Div, 91(9),* 1249-1274.

Sherif, M. A., Ishibashi, I., & TSUCHIYA, C. (1978). Pore-pressure prediction during earthquake loadings. *Soils and Foundations, 18(4),* 19-30.

Sivathayalan, S. (1994). *Static, cyclic and post liquefaction simple shear response of sands*. University of British Columbia.

Towhata, I., & Ishihara, K. (1985). Shear work and pore water pressure in undrained shear. *Soils and Foundations, 25(3),* 73-84.

Tsuha, C. H. C., Foray, P., Jardine, R., Yang, Z., Silva, M., & Rimoy, S. (2012). Behaviour of displacement piles in sand under cyclic axial loading. *Soils and foundations, 52(3),* 393-410.

Vaid, Y. P., Stedman, J., & Sivathayalan, S. (2001). Confining stress and static shear effects in cyclic liquefaction. *Canadian Geotechnical Journal, 38(3),* 580-591.

Vaid, Y. P., & Chern, J.-C. (1983). Effect of static shear on resistance to liquefaction. *Soils and Foundations, 23(1),* 47-60.

Vaid, Y. P., & Negussey, D. (1984). Relative density of pluviated sand samples. *Soils and Foundations, 24(2),* 101-105.

Wang, J.; Guo, L., Cai, Y.-Q., Xu, C.-J. & Gu, C. (2013a) Strain and pore pressure development on soft marine clay in triaxial tests with a large number of cycles. *Ocean Engineering*, 74:125–132

Wang, J.; Cai, Y.-Q. & Yang, F, (2013b) Effects of Initial Shear Stress on Cyclic Behavior of

Saturated Soft Clay, *Marine Georesources & Geotechnology*, 31(1):86–106

Wang, J., Liu, F.-Y., Wang, P, & Cai, Y.-Q., (2016) Particle size effects on coarse soil-geogrid interface response in cyclic and post-cyclic direct shear tests，*Geotextiles and Geomembranes*，44(6): 854-861

Wichtmann, T., & Triantafyllidis, T. (2016a). An experimental data base for the development, calibration and verification of constitutive models for sand with focus to cyclic loading: part I—tests with monotonic loading ans stress cycles. *Acta Geotechnica, 11(4),* 739-761.

Wichtmann, T., & Triantafyllidis, T. (2016b). An experimental data base for the development, calibration and verification of constitutive models for sand with focus to cyclic loading: part II —tests with strain cycles and combined loading. *Acta Geotechnica, 11(4),* 763-774.

Yang, J., & Sze, H. (2011). Cyclic behaviour and resistance of saturated sand under non-symmetrical loading conditions. *Géotechnique,61(1),*59-73.

Yang, Z., Jardine, R., Zhu, B., Foray, P., & Tsuha, C. (2010). Sand grain crushing and interface shearing during displacement pile installation in sand. *Géotechnique, 60(6),* 469-482.

Yang, Z., & Pan, K. (2017). Flow deformation and cyclic resistance of saturated loose sand considering initial static shear effect. *Soil Dynamics and Earthquake Engineering, 92(2017),* 68-78.

Yin, Z.-Y., Chang, C.S., Hicher, P.Y. (2010). Micromechanical modelling for effect of inherent anisotropy on cyclic behaviour of sand. Int. J. Solids Struct., 47(14-15): 1933-1951.

Yin, Z.-Y., Xu, Q., Chang, C.S. (2013). Modeling cyclic behavior of clay by micromechanical approach. ASCE J. Eng. Mech., 139(9), 1305–1309.

Yin, Z.-Y., Wu, Z.Y., Hicher, P.Y. (2018). Modeling the monotonic and cyclic behavior of granular materials by an exponential constitutive function. J. Eng. Mech. ASCE, 144(4): 04018014.

Yoshimine, M., Ishihara, k., & Vargas, W. (1998). Effects of principal stress direction and intermediate principal stress on undrained shear behavior of sand. *Soils and Foundations, 38(3),* 179-188.

Yoshimine, M., Robertson, P., & Wride, C. (1999). Undrained shear strength of clean sands to trigger flow liquefaction. *Canadian Geotechnical Journal, 36(5),* 891-906.

Tables

Table 1 Physical properties of standard Fontainebleau

Grain shape	S_iO_2: %	D_{50}(mm)	$C_u(D_{60}/D_{10})$	G_s	e_{max}	e_{min}
Sphericity	99.70	0.21	1.53	2.65	0.882	0.510

Table 2 Summary of experiments on tested Fontainebleau sand

Test No.	Loading type		e_0	D_{r0} %	σ'_{n0} (kPa)	τ_{pt} (kPa)	τ_{ave} (kPa)	τ_{cyc} (kPa)	τ_{ave}/σ'_{n0}	CSR	N_L
m1	Monotonic		0.744	37.1	104	6.6	-	-	-	-	-
m2	Monotonic		0.688	52.2	104	12.8	-	-	-	-	-
m3	Monotonic		0.631	67.5	104	16.1	-	-	-	-	-
m4	Monotonic		0.586	79.6	104	25	-	-	-	-	-
m5	Monotonic		0.644	64.0	208	28.1	-	-	-	-	-
m6	Monotonic		0.733	40.1	312	26	-	-	-	-	-
m7	Monotonic		0.730	40.9	312	25.5	-	-	-	-	-
m8	Monotonic		0.679	54.6	312	34	-	-	-	-	-
m9	Monotonic		0.627	68.5	312	44	-	-	-	-	-
m10	Monotonic		0.617	71.2	312	59	-	-	-	-	-
m11	Monotonic		0.615	71.8	312	60	-	-	-	-	-
m12	Monotonic		0.651	62.1	416	69	-	-	-	-	-
c13	Symmetrical loading		0.658	60.2	104	14	0	5.2	0	0.05	18
c14	Symmetrical loading		0.664	58.6	208	27	0	5.2	0	0.025	88
c15	Symmetrical loading		0.670	57.0	208	26	0	10.4	0	0.05	14
c16	Symmetrical loading		0.660	59.7	208	28	0	20.8	0	0.1	2
c17	Symmetrical loading		0.663	58.9	312	42	0	15.6	0	0.05	33
c18	Symmetrical loading		0.662	59.1	416	57	0	10.4	0	0.025	366
c19	Symmetrical loading		0.660	59.7	416	57	0	10.4	0	0.025	300
c20	Symmetrical loading		0.638	65.6	416	67	0	20.8	0	0.05	81
c21	Symmetrical loading		0.663	58.9	416	57	0	20.8	0	0.05	62
c22	Symmetrical loading		0.656	60.8	416	60	0	20.8	0	0.05	62
c23	Symmetrical loading		0.655	61.0	416	60	0	31.2	0	0.075	10
c24	Symmetrical loading		0.644	64.0	416	65	0	41.6	0	0.1	3
c25	Symmetrical loading		0.648	62.9	416	65	0	62.4	0	0.167	1
c26	Non-symm	stress reversal	0.629	68.0	416	71	5.2	10.4	0.0125	0.025	600
c27	Non-symm	stress reversal	0.654	61.3	416	60	5.2	20.8	0.0125	0.05	57
c28	Non-symm	Non-stress reversal	0.669	57.3	416	53	10.4	10.4	0.025	0.025	368
c29	Non-symm	stress reversal	0.663	58.9	416	56	10.4	20.8	0.025	0.05	19
c30	Non-symm	stress reversal	0.654	61.3	416	60	10.4	20.8	0.025	0.05	39
c31	Non-symm	stress reversal	0.641	64.8	416	66	10.4	20.8	0.025	0.05	56
c32	Non-symm	Non-stress reversal	0.653	61.6	416	61	20.8	10.4	0.05	0.025	240
c33	Non-symm	Non-stress reversal	0.641	64.8	416	57	20.8	10.4	0.05	0.025	310
c34	Non-symm	Non-stress reversal	0.635	66.4	416	71	20.8	20.8	0.05	0.05	100
c35	Non-symm	Non-stress reversal	0.666	58.1	416	55	20.8	20.8	0.05	0.05	45
c36	Non-symm	Stress reversal	0.640	65.1	416	66	20.8	41.6	0.05	0.1	7
c37	Non-symm	Non-stress reversal	0.654	61.3	416	60	41.6	10.4	0.1	0.025	330
c38	Non-symm	Non-stress reversal	0.664	58.6	416	56	41.6	20.8	0.1	0.05	19

* Initial void ratio e_0 and relative densities D_{r0} were measured at the corresponding initial effective normal stress σ'_{n0}; for monotonic loading, the shear stress at phase transformation state τ_{pt} was measured based on the experimental results, and for cyclic loading τ_{pt} was calculated based on the empirical equation Eq. (2); cyclic shear stress ratio CSR could be expressed by the cyclic shear stress τ_{cyc} over the initial effective normal stress σ'_{n0}; N_L is the number of cycles to liquefaction.

Table 3 Physical properties of three studied sands

Material	D_{50} (mm)	C_u	G_s	e_{max}	e_{min}
Fraser River sand	0.30	1.6	2.72	1.000	0.680
Quiou sand	0.65	2.8	2.70	1.169	0.763
Karlsruhe sand	0.14	1.5	2.70	1.054	0.677

Table 4 Parameters of Eqs. (2) and (6) with different sands

Material	α	β	ϕ_{pt} (°)	μ	ψ
Fontainebleau sand	0.68	1.76	24	1.396	3.505
Fraser River sand	1.233	1.478	30	3.183	2.787
Quiou sand	0.767	0.318	27	1.004	4.353
Karlsruhe sand	0.738	0.746	29.6	1.498	4.764

Table 5 Summary of additional tests on Fontainebleau sand (σ'_{n0} = 500kPa)

Test No.	e_0	τ_{ave} (kPa)	τ_{cyc} (kPa)	τ_{ave}/σ'_{n0}	CSR	τ_{pt} (kPa)	N_L
B1	0.619	0	12.5	0	0.025	85.5	1015
B2	0.626	0	25	0	0.05	81.6	74
B3	0.612	0	50	0	0.1	89.6	4
B4	0.613	12.5	25	0.025	0.05	89.0	64
B5	0.609	25	25	0.05	0.05	91.3	36
B6	0.619	50	25	0.1	0.05	85.5	1

Figure captions

Figure 1 ~~Laboratory test model of pile~~ Analysis of soil element adjacent to pile based on simple shear apparatus

Figure 2 ~~Particle shape of Fontainebleau sand~~ Details of specimens preparation: (a) particle shape of Fontainebleau sand, (b) air-pluviation technique, (c) sand specimen

Figure 3 Undrained monotonic test results on Fontainebleau sand: (a) γ-τ with different e_0; (b) σ'_n -τ with different e_0; (c) γ-τ with differentσ'_{n0}; (d) σ'_n -τ with different σ'_{n0}; (e) σ'_n/σ'_{n0} -τ/τ_{pt} with different e_0 ; (f) σ'_n/σ'_{n0} -τ/τ_{pt} with different σ'_{n0}

Figure 4 τ_{pt} as a function of experimental variables σ'_{n0} and D_{r0}: (a) τ_{pt} - D_{r0}; (b) τ_{pt}/σ'_{n0}- D_{r0}

Figure 5 Symmetrical cyclic response of Fontainebleau sand: (a)σ'_n-τ, (b) γ-τ, (c) N_{cyc}-τ, (d) N_{cyc}-σ'_n

Figure 6 Degradation of effective normal stress under different CSRs: (a)σ'_{n0}=104 kPa; (b) σ'_{n0}=208 kPa; (c)σ'_{n0}=314 kPa; (d) σ'_{n0}=416 kPa

Figure 7 Number of cycles to liquefaction as a function of the normalized cyclic shear stress τ_{cyc}/τ_{pt}

Figure 8 Non-symmetrical cyclic response of Fontainebleau sand with stress reversal loading: (a)σ'_n-τ, (b) γ-τ, (c) N_{cyc}-τ, (d) N_{cyc}-σ'_n

Figure 9 Non-symmetrical cyclic response of Fontainebleau sand with no-stress reversal loading: (a)σ'_n-τ, (b) γ-τ, (c) N_{cyc}-τ, (d) N_{cyc}-σ'_n

Figure 10 Degradation of effective normal stress under different average shear stress τ_{ave}: (a) τ_{ave} = 5.2 kPa; (b) τ_{ave} = 10.4 kPa; (c) τ_{ave} = 20.8 kPa; (d) τ_{ave} = 41.6 kPa

Figure 11 Evaluation of effective residual normal stress in no-stress reversal cyclic loading: (a) hysteresis loops of instability; (b) fitting line for residual effective normal stress

Figure 12 Cyclic resistance surface for cyclic simple shear tests on Fontainebleau sand

Figure 13 Cyclic resistance diagram for cyclic simple shear tests on Fontainebleau sand: (a) relationship between τ_{cyc}/τ_{pt} and τ_{ave}/τ_{pt}; (b) relationship between K and N_L

Figure 14 Normalized effective normal stress against normalized number of cycles to liquefaction

Figure 15 Calibration procedure for the degradation of the effective normal stress

Figure 16 Eq. (2) calibration procedure: (a) Fraser River sand; (2) Quiou sand; (3) Karlsruhe sand

Figure 17 Eq. (6) calibration procedure: (a) Fraser River sand; (2) Quiou sand; (3) Karlsruhe sand

Figure 18 Comparisons between simulations and experiments on Fontainebleau sand: (a) training tests; (b) additional tests

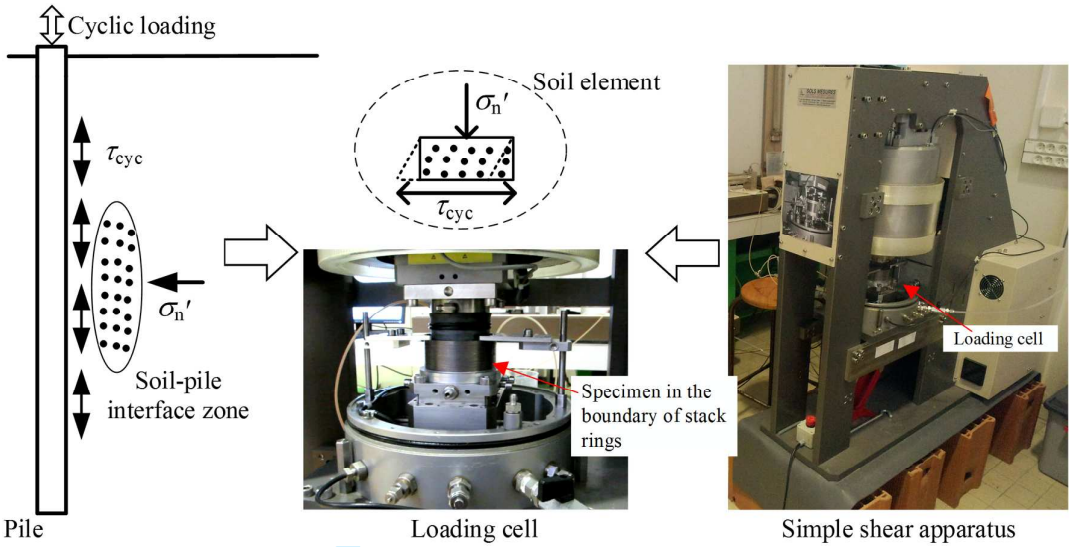

Figure 1

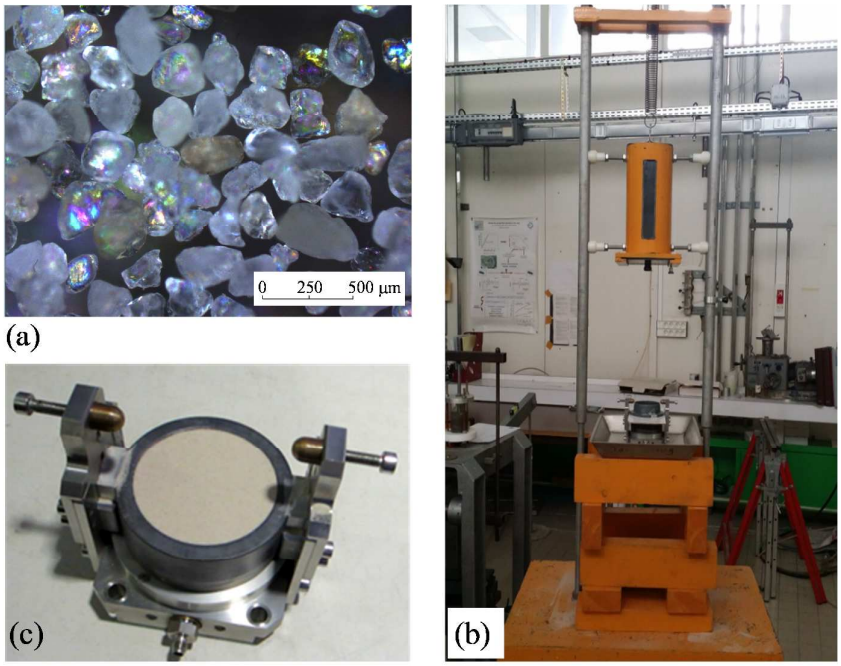

Figure 2

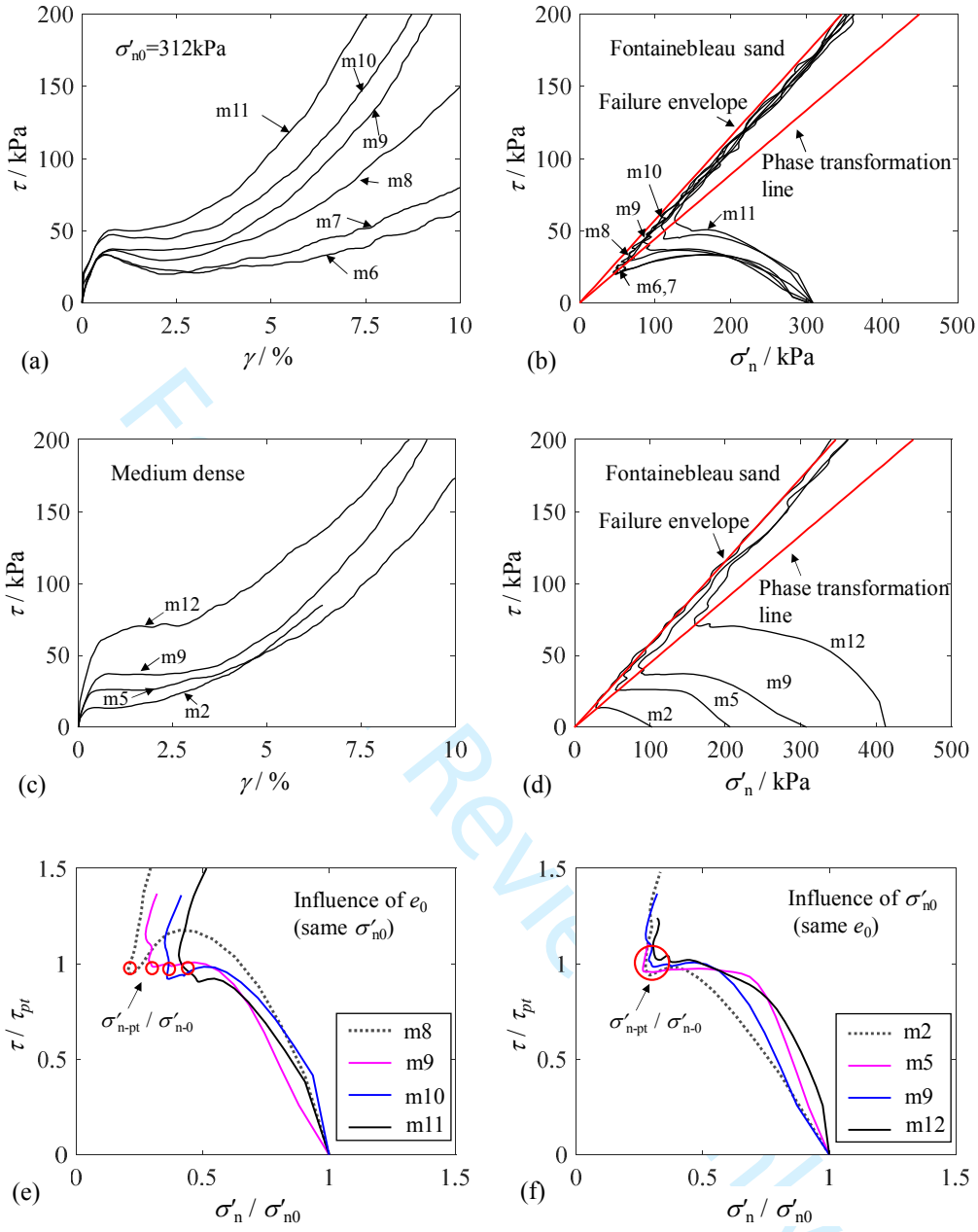
σ'n0=312kPa
m10
m11
m9
m8
m7
m6
τ / kPa
γ / %
(a)
Fontainebleau sand
Failure envelope
Phase transformation line
m10
m9
m8
m11
m6,7
σ'n / kPa
(b)
Medium dense
m12
m9
m5
m2
(c)
Fontainebleau sand
Failure envelope
Phase transformation line
m12
m9
m5
m2
(d)
Influence of e0
(same σ'n0)
σ'n-pt / σ'n-0
m8
m9
m10
m11
τ / τpt
σ'n / σ'n0
(e)
Influence of σ'n0
(same e0)
σ'n-pt / σ'n-0
m2
m5
m9
m12
(f)

Figure 3

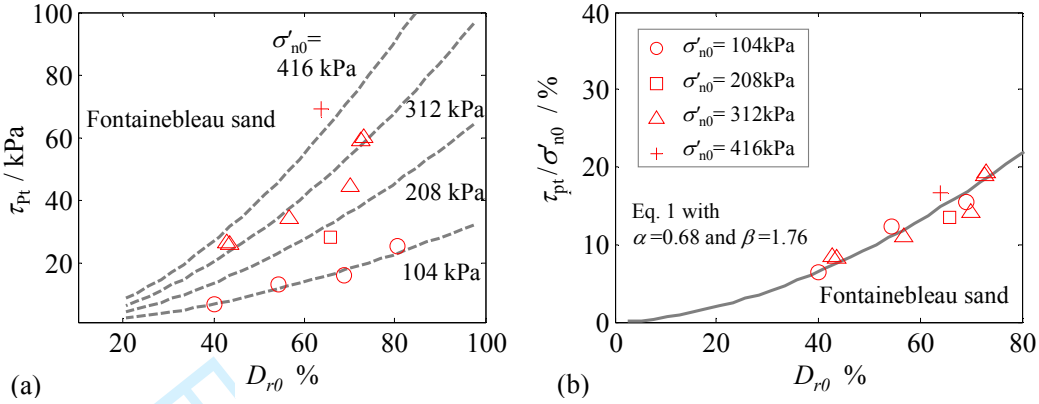

Figure 4

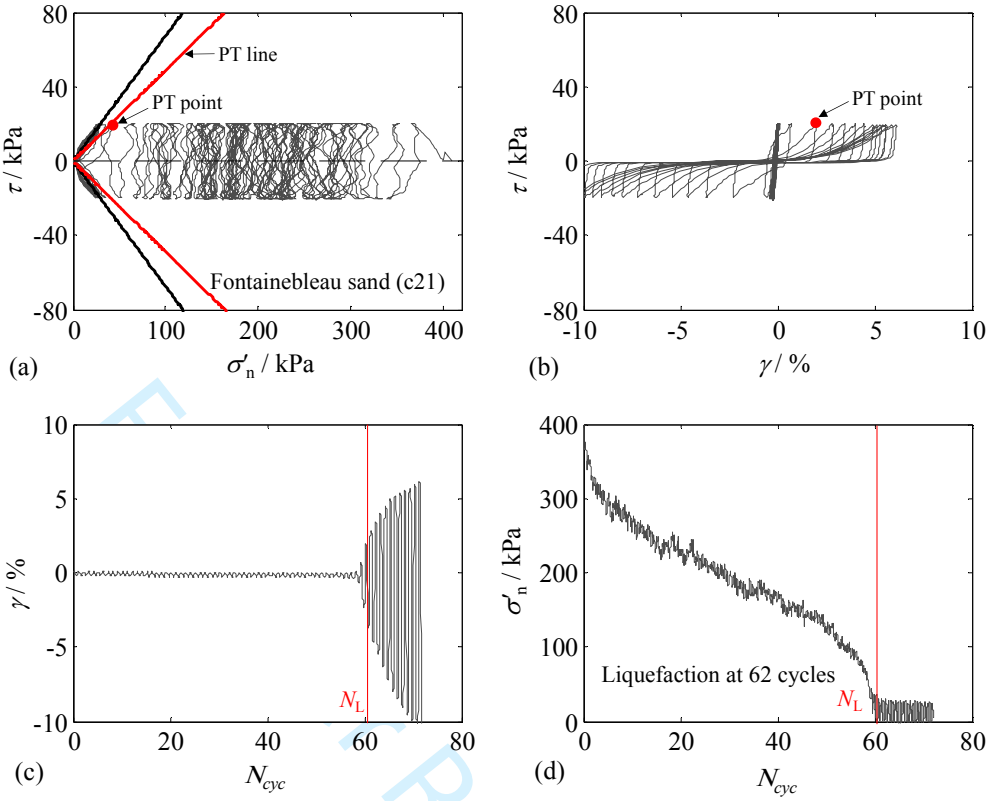

Figure 5

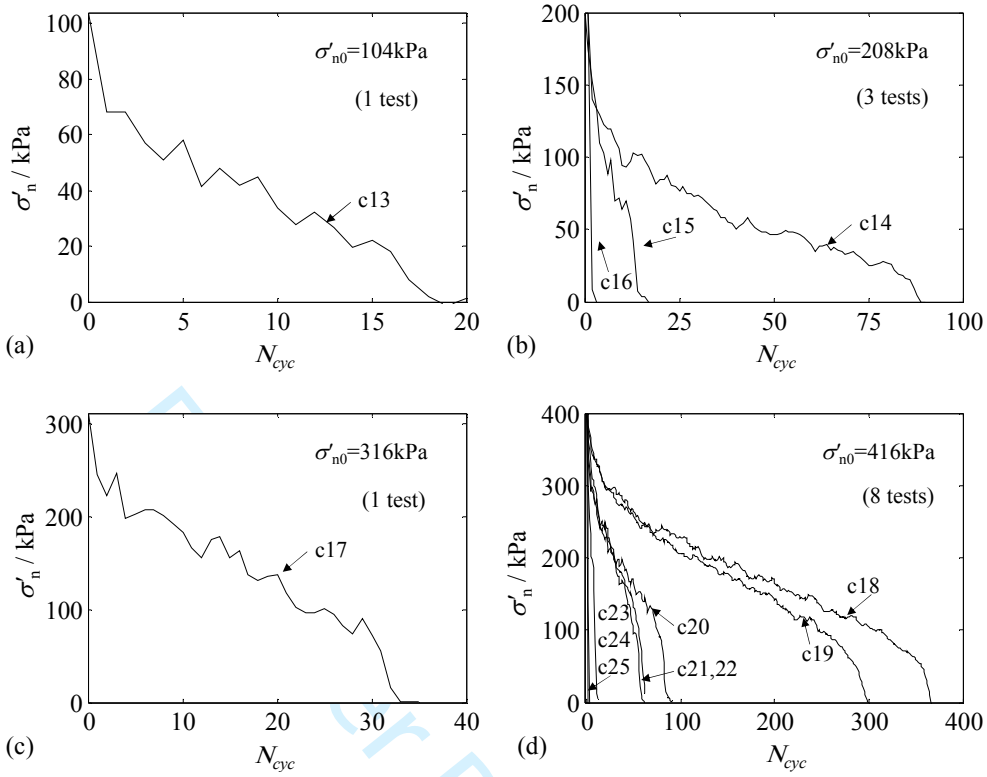
σ'n0=104kPa
(1 test)
c13
σ'n / kPa
Ncyc
(a)
σ'n0=208kPa
(3 tests)
c14
c15
c16
(b)
σ'n0=316kPa
(1 test)
c17
(c)
σ'n0=416kPa
(8 tests)
c18
c19
c20
c21,22
c23
c24
c25
(d)

Figure 6

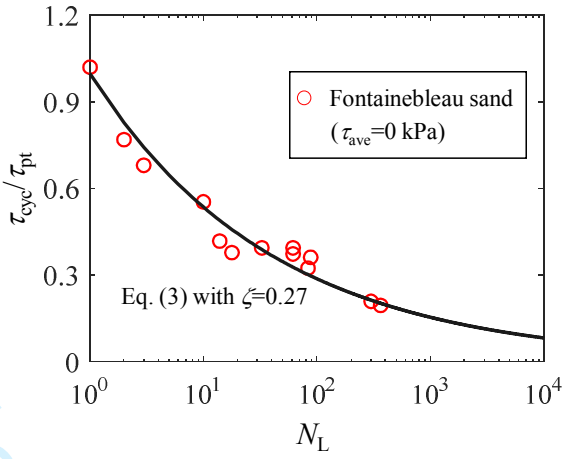

Figure 7

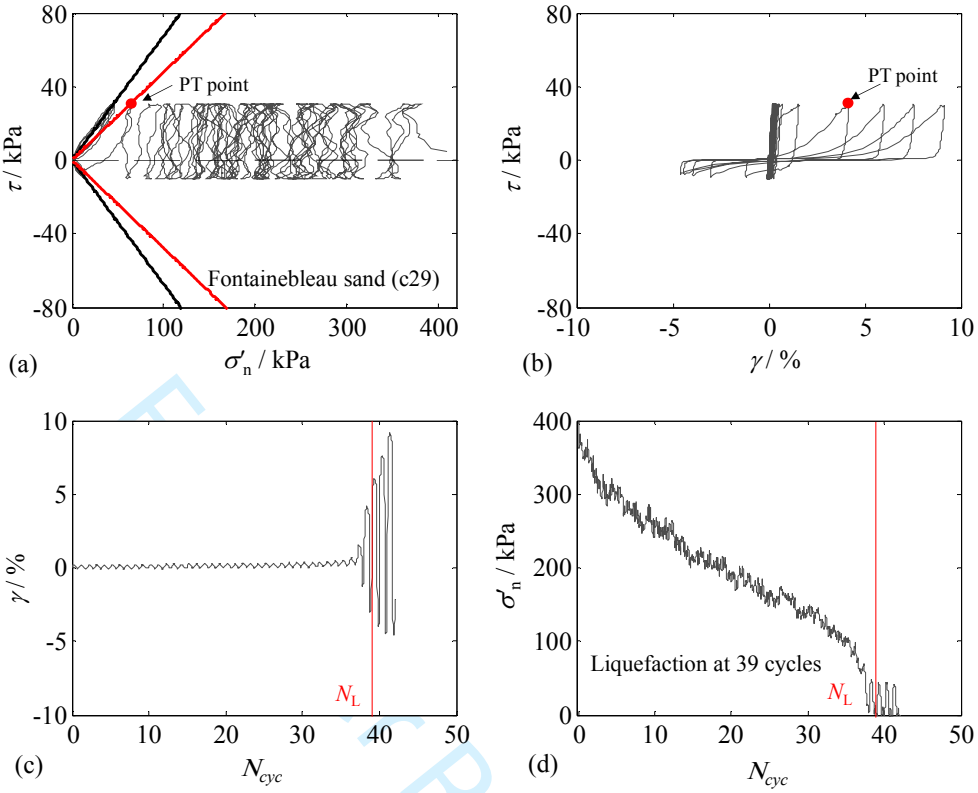
PT point
Fontainebleau sand (c29)
τ / kPa
σ'n / kPa
(a)
PT point
τ / kPa
γ / %
(b)
γ / %
NL
Ncyc
(c)
σ'n / kPa
Liquefaction at 39 cycles
NL
Ncyc
(d)

Figure 8

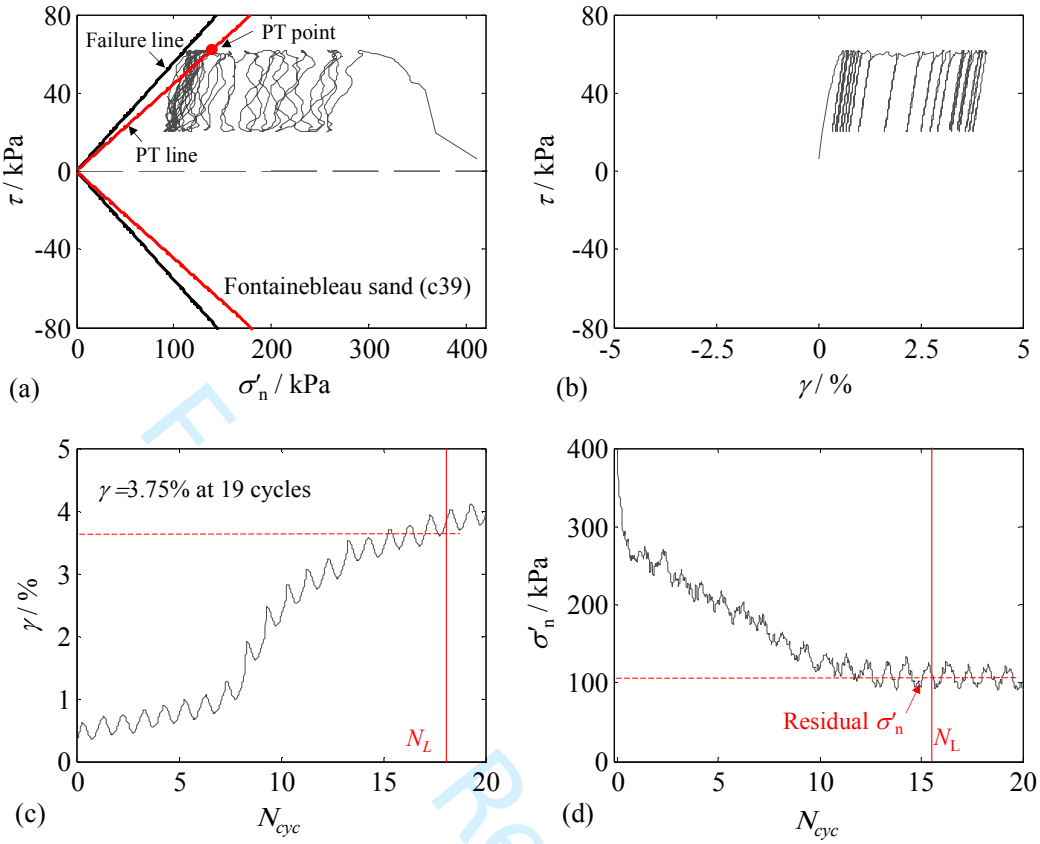
Failure line
PT point
PT line
Fontainebleau sand (c39)
τ / kPa
σ'n / kPa
(a)
γ / %
(b)
γ =3.75% at 19 cycles
NL
Ncyc
(c)
σ'n / kPa
Residual σ'n
NL
Ncyc
(d)

Figure 9

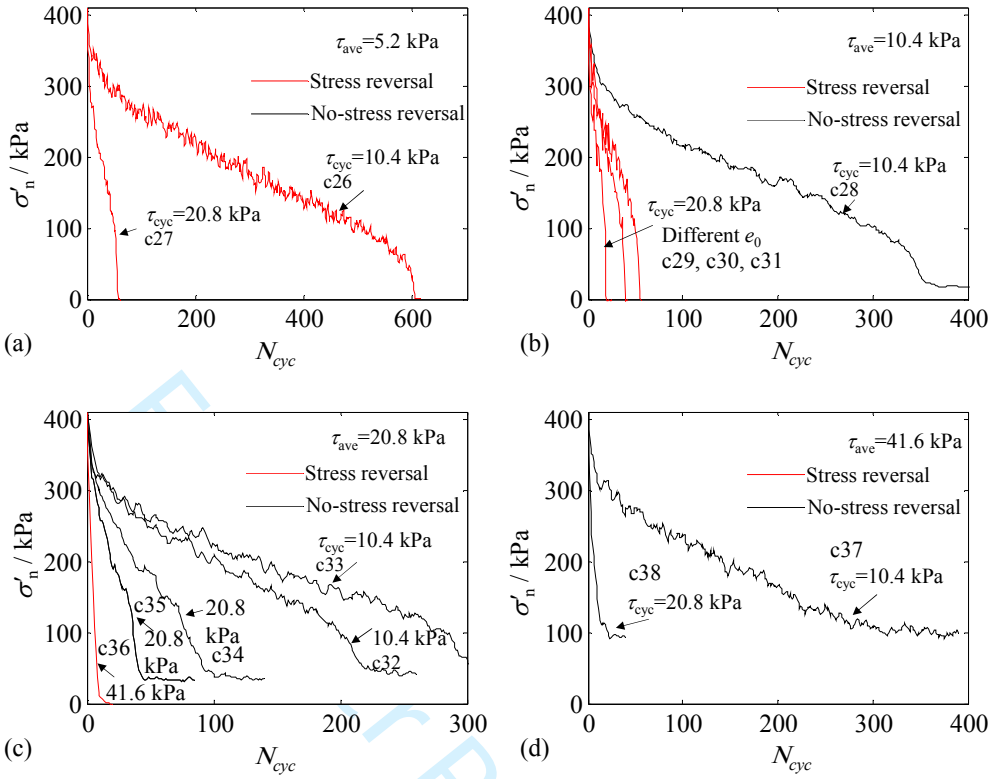

Figure 10

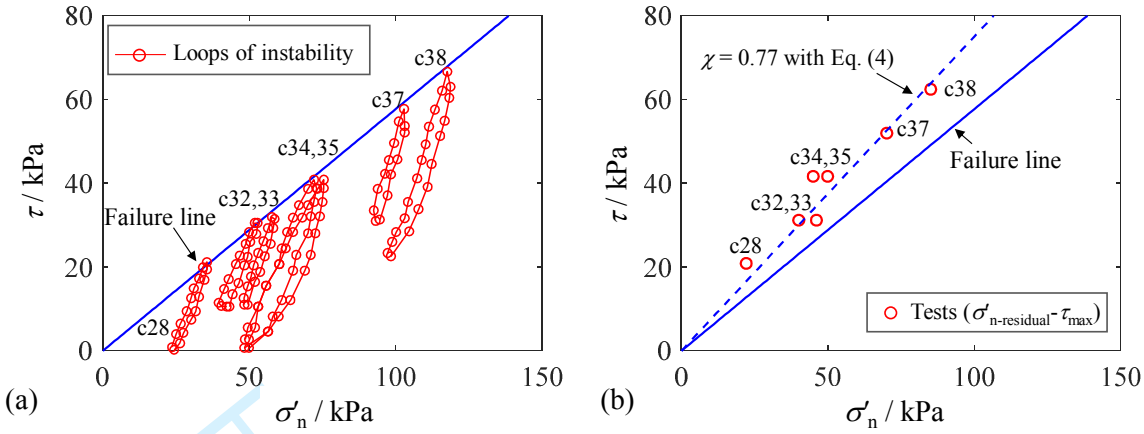

Figure 11

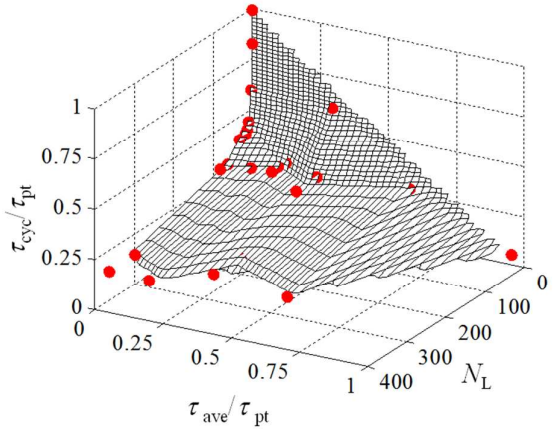

Figure 12

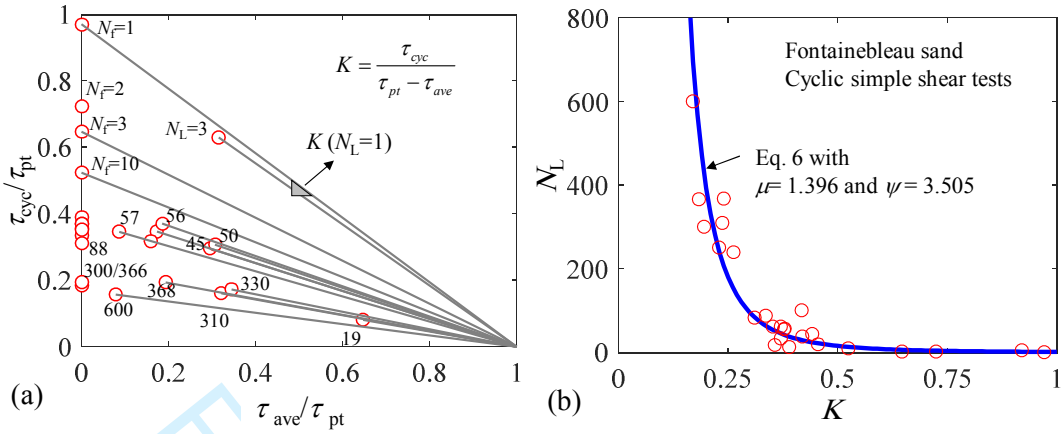

Figure 13

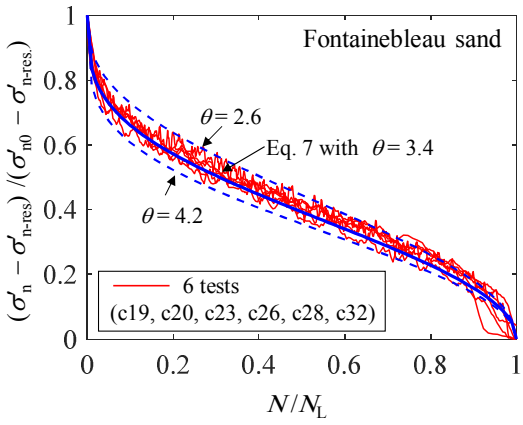

Figure 14

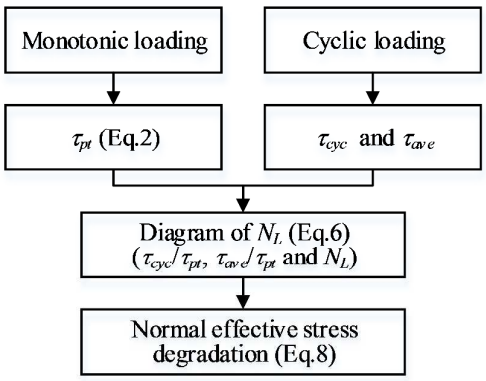

Figure 15

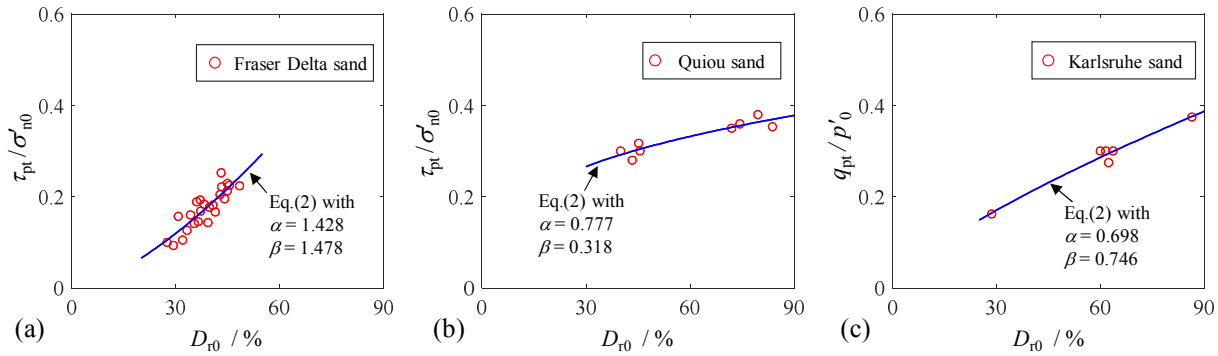

Figure 16

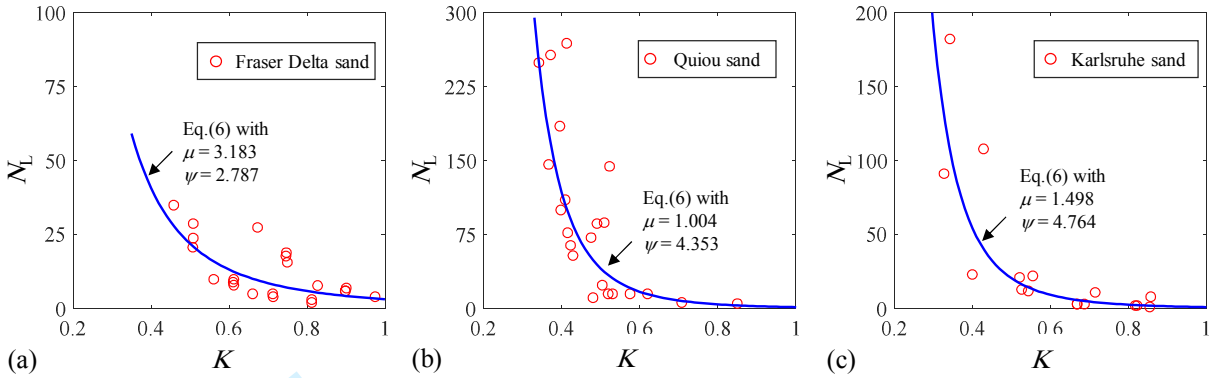

Figure 17

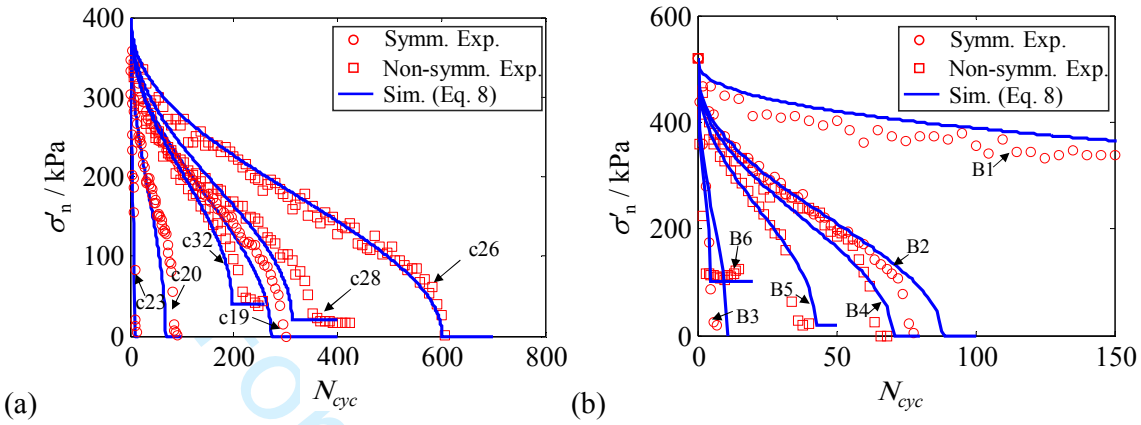

Figure 18